Chapter 4

Results

4.1 Heterostructure Hot-Electron Diode

4.1.1 The Data Sets Examined

The data samples[1] are outputs of computer simulations of the dynamics of the generic model with one spatial coordinate (equations 2.8 and 2.9, see 2.1). The initial condition is a cosine wave in the spatial coordinate. This makes sure that simulations using identical parameter sets always lead to the same stationary dynamics. The computer simulations were made for a system with a spatial extent of 40 units. The spatio-temporal current at the interface layer (in dimensionless units) was recorded at 25 locations during the simulations. The sampling intervals are denoted with Δ_x and Δ_t in what follows. They are $\Delta_x = 1.6$ and $\Delta_t = 0.1$ in dimensionless units[2]. The global data (the mean current across the HHED) was recorded with the same sampling rate as the spatio-temporal data.

The parameters used (cf. table 4.1) were $\alpha = 0.35$, $j_0 = 1.24$ for data set E and $\alpha = 0.35$, $j_0 = 1.31$ for data set F.

abbreviation	j_0	type of dynamics
E	1.24	periodic (periodic spiking)
F	1.31	temporal chaos (chaotic spiking)

Table 4.1: **Abbreviations for the data sets examined.**

An overview of the stationary dynamics obtained for different parameter sets is given in figure 4.1. Data set E belongs to the dark region of periodic spiking on the left half of

[1]All data samples for this system are courtesy of Dipl. Phys. Sumit Bose.

[2]For details about the integration of the partial differential equations using an adaptive stepsize Runge-Kutta scheme see [15].

the plot. Data set F belongs to the small region of chaotic spiking lying approximately in the center of the plot.

Both data sets were recorded after the transient.

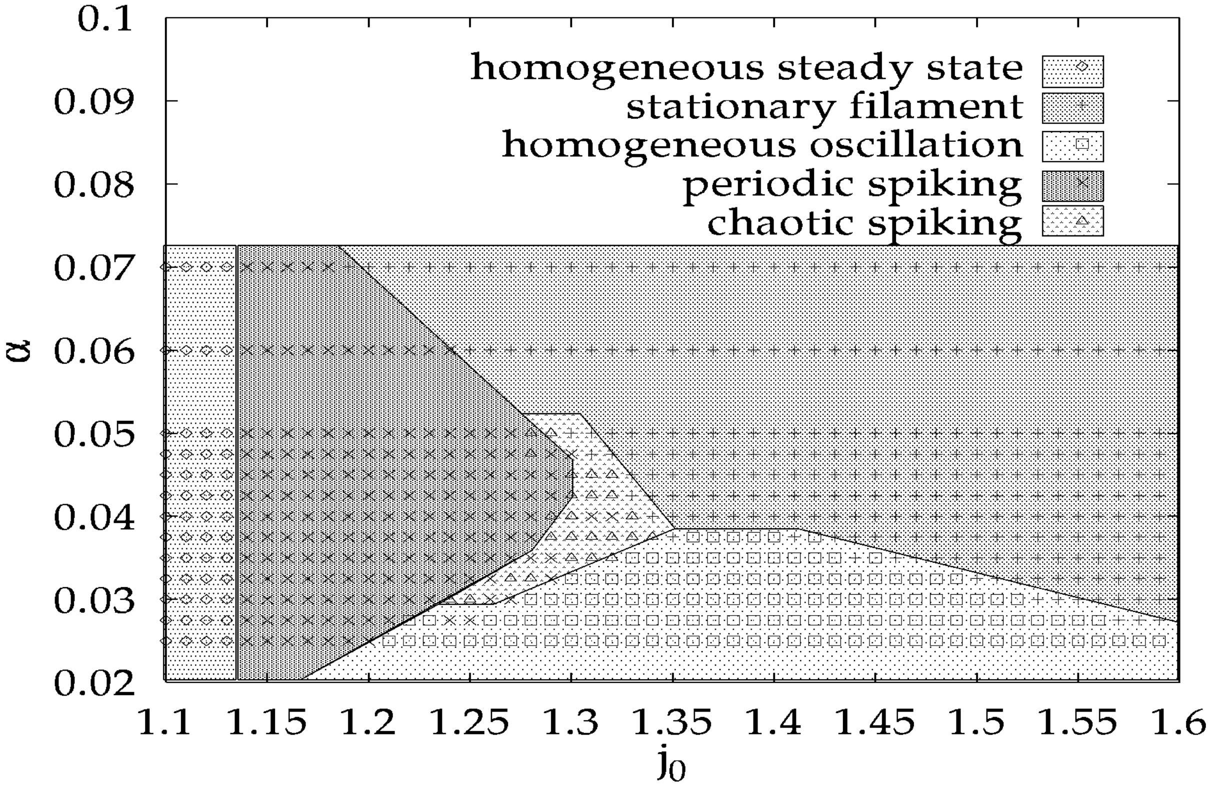

Figure 4.1: **Phase diagram for the HHED system in the parameter space.** *(From: [15] p.34).*

4.1.2 Analysis of the Global Data

Figures 4.2 and 4.4 show the global data sets E and F. The quantity recorded is the mean current through the interface layer. The oscillations between the spikes are damped for the periodic data while they are undamped for data set F. First some classical methods of data analysis are applied to characterise the data.

The spectrum of data set E (figure 4.3) clearly belongs to a purely periodic signal with harmonics. The continuous parts of the power spectrum of system F (figure 4.5, note the linear scale) indicate chaos as there are no stochastic components in the data.

The autocorrelation function of the global data set F (figure 4.6) decreases in the typical time between two spikes. Apparently the information about the phase is lost during the occurrence of the spikes. For greater lags a certain correlation remains, the autocorrelation coefficients do not seem to decrease any further.

The histogram for the data set E (figure 4.8) consists of two characteristic parts. The boxes far from the mean value (box numbers 0...$\approx$65 and $\approx$120...200) with low relative frequencies correspond to the spikes. Their non-symmetry reflects the fact that the upper half of the spikes lasts shorter than the lower half. The boxes located around the mean value are the result of the damped oscillations between the spikes. The very clear shape of this histogram is typical for a strictly periodic signal without noise. The undamped oscillation between the spikes in the global data set F is responsible for the main part of the histogram shown in figure 4.9. A similar shape would be found for a strictly periodical oscillation[3], only the fluctuations of the values indicate the chaotic behavior here. Such fluctuations could in principle result from a small number of samples, but here both sets of global data consist of an equal number of samples[4].

The maximum map of data set F is shown in figure 4.10. The non-interpolated local minima in the data were used for this plot. The structure of the point cloud seems to have a dimension close to one. This indicates an attractor dimension for F that is close to two.

Its form suggests to consider it as the plot of a function that is iterated by the dynamics[5]. The unstable fixed point that lies approximately at (0.2,0.2) corresponds to the rather periodic oscillations between the spikes. The regions of the curve with great slopes belong to parts of the dynamics where a perturbation will be amplified very much, these are parts close to the onset of the spikes. Any small increase in the minimum value indicates the immediate occurrence of a spike. The lower part of the maximum map with small slopes corresponds to the first minimum after the spikes. The nearly horizontal part of the curve on the left side of the plot corresponds to the second minimum after the spikes. Here the oscillation begins again. In that region a perturbation will be almost wiped out.
(A discussion of strongly nonuniform dynamics can be found in [43]).

---

[3] Cf. chapter 3.2.5.

[4] They consist of 20971 samples.

[5] Cf. chapter 3.3.2.

The attractor reconstructions also allow the recognition of the different parts of the dynamics: Figure 4.11 (left) shows the reconstruction[6] for data set E. The damped oscillations between the spikes lead to the spiral-like part in the center of the plot. The spiking corresponds to the line leading from the innermost part of the spiral around it and back on its outside.

The oscillations between the spikes of data set F are undamped, instead of a spiral a cycle-like structure is found in the attractor reconstruction (figure 4.11, right). The onset of the spikes starts from all locations of the cycle with approximately the same probability[7]. The motion then leads around the cycle and then back into almost the same location for all spikes. This corresponds to the thin peak-like structure on the lower left that leads back into the cycle[8].

For data set F the dimension of the attractor was estimated using the nearest neighbor[9] program package by Kostelich et al. (cf. [47]). The results for different embedding dimensions, delay times and nearest neighbor orders are shown in figure 4.1.2. They are all significantly smaller than two. As for a chaotic system the attractor dimension must be greater than two the estimated values must be considered as meaningless[10]. The reason for the wrong estimates computed by the nearest neighbor algorithm is that the attractor is very inhomogeneous.

The completely wrong dimension estimates for a system without noise where it is known that the attractor dimension is very low again show that the output of such procedures must be interpreted with greatest care. It is always necessary to be 'familiar' with the data and look at Poincaré sections and attractor reconstructions before one tries to make dimension estimates.

The dimension of the attractor corresponding to data set E, a limit cycle, is of course one.

The Lyapunov dimension, which is an upper limit for the fractal dimension, has been calculated in [15] (p.55) for different values of j_0 (and $\alpha = 0.35$). The result for the parameter set corresponding to data set F is $D_L = 2.085$.

It was tried to estimate the Lyapunov exponents for data set F with the programs 'eck' and 'expons' by E.J.Kostelich (cf. [50]). As the resulting set of Lyapunov exponents always leads to Kaplan Yorke dimensions smaller than two the obtained values must be considered as spurious. The reason for the apparently false estimates may again lie the inhomogeneity of the attractor.

[6] The delay time used is $5 \cdot \Delta_t$.

[7] Corresponding to the almost vertical segment in the maximum map.

[8] Corresponding to the almost horizontal segment in the maximum map.

[9] Cf. chapter 3.4.2.

[10] Except that they indicate a dimension close to two.

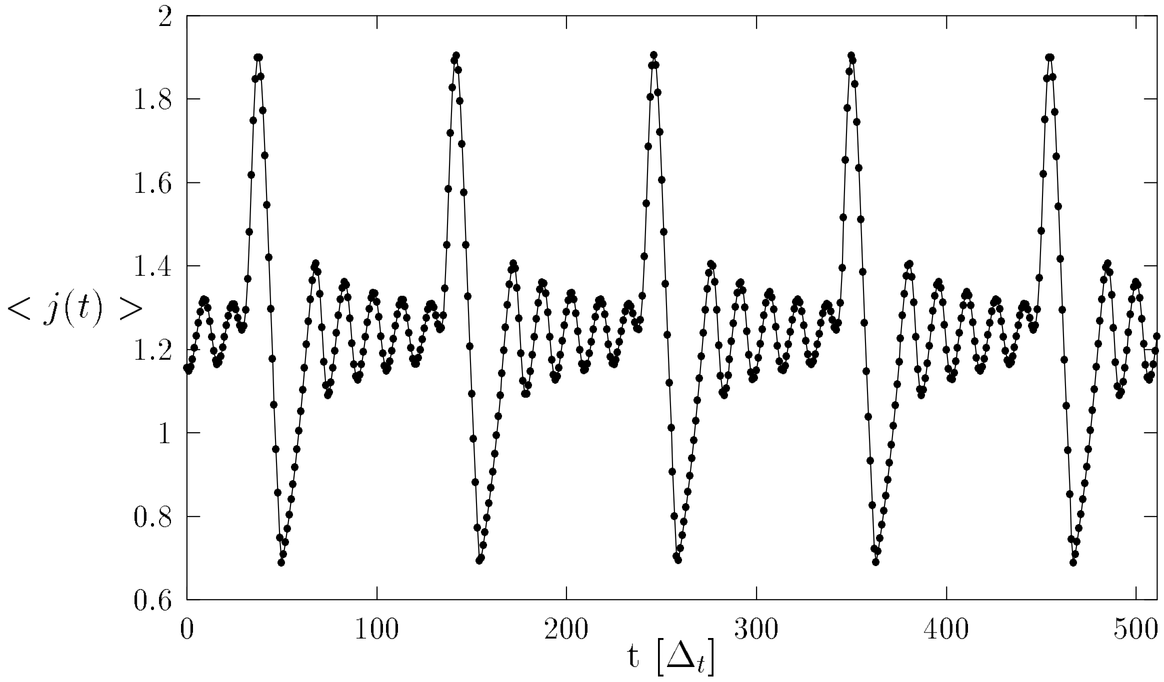

Figure 4.2: **Plot of the global data set E (dimensionless units).**

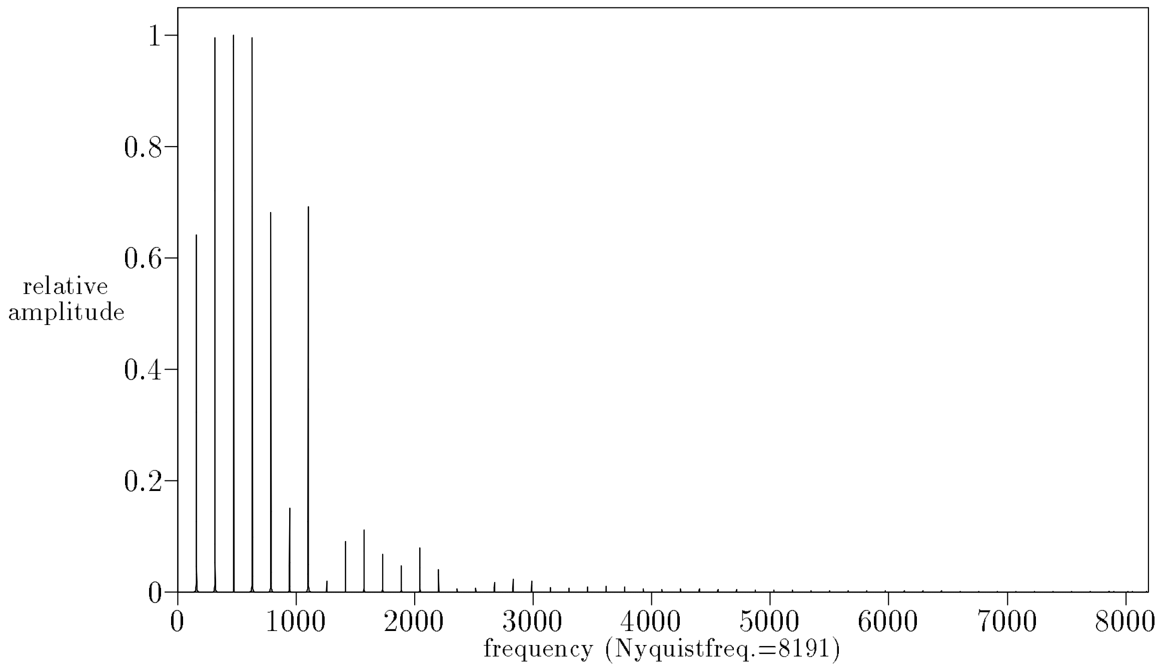

Figure 4.3: **Spectrum of the global data set E.**
The behavior is purely periodic with harmonics.

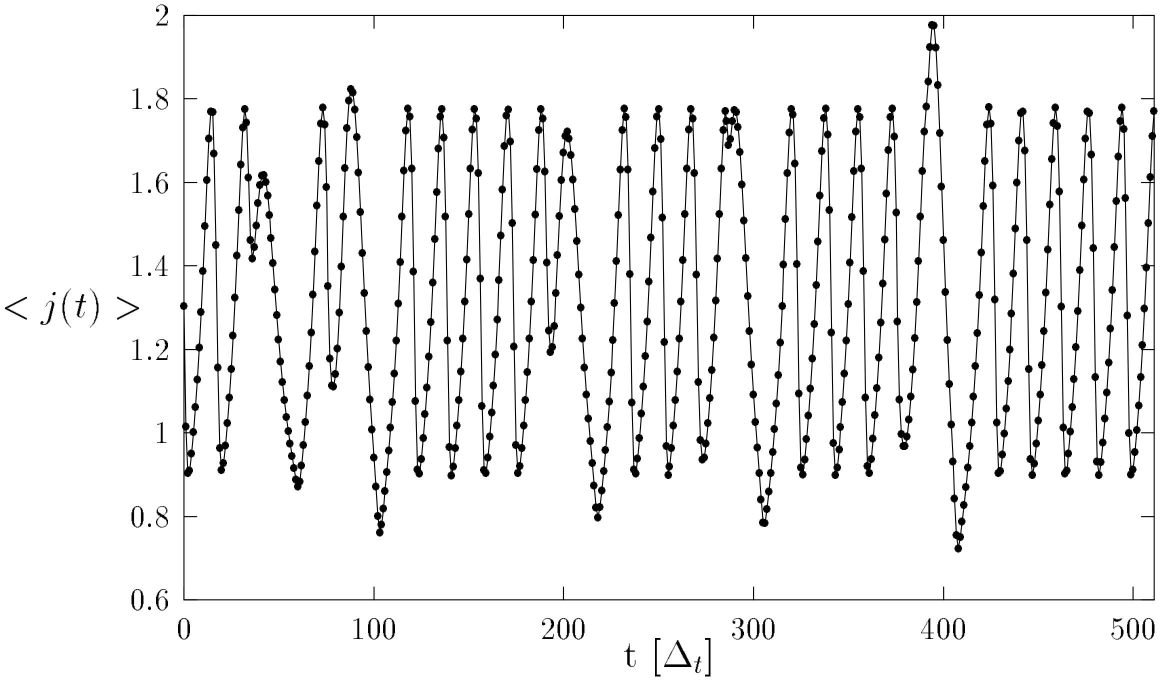

Figure 4.4: **Plot of the global data set F (dimensionless units).**

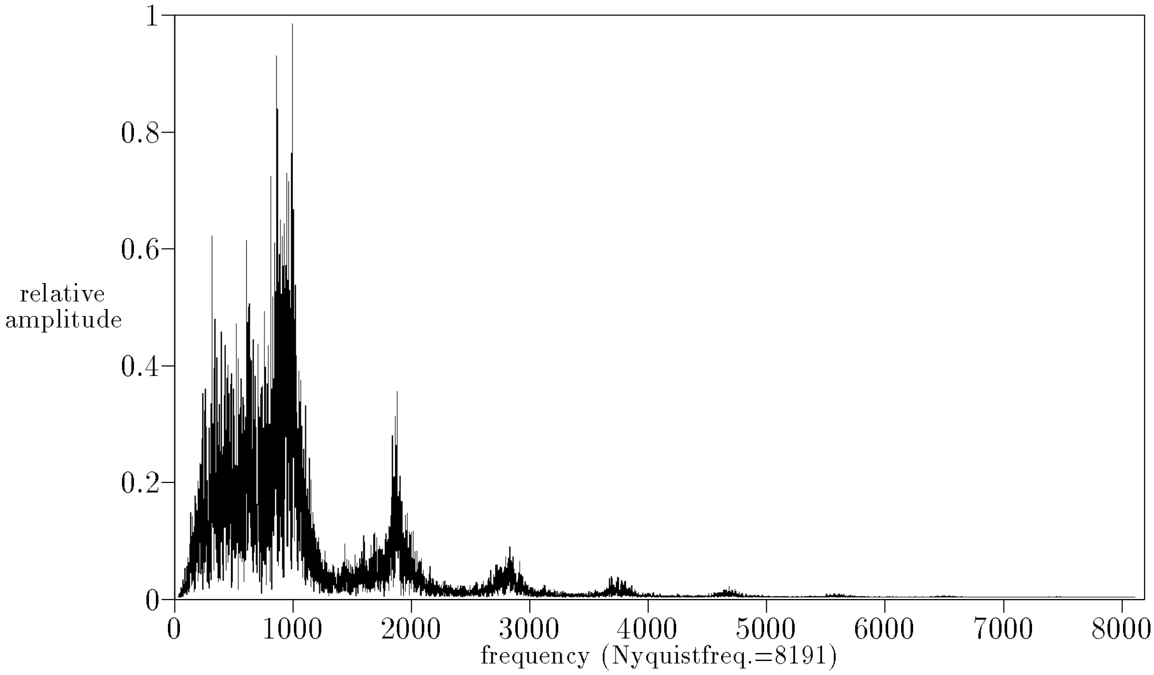

Figure 4.5: **Spectrum of the global data set F.**
The continuous spectrum suggests chaotic dynamics for this parameter set.

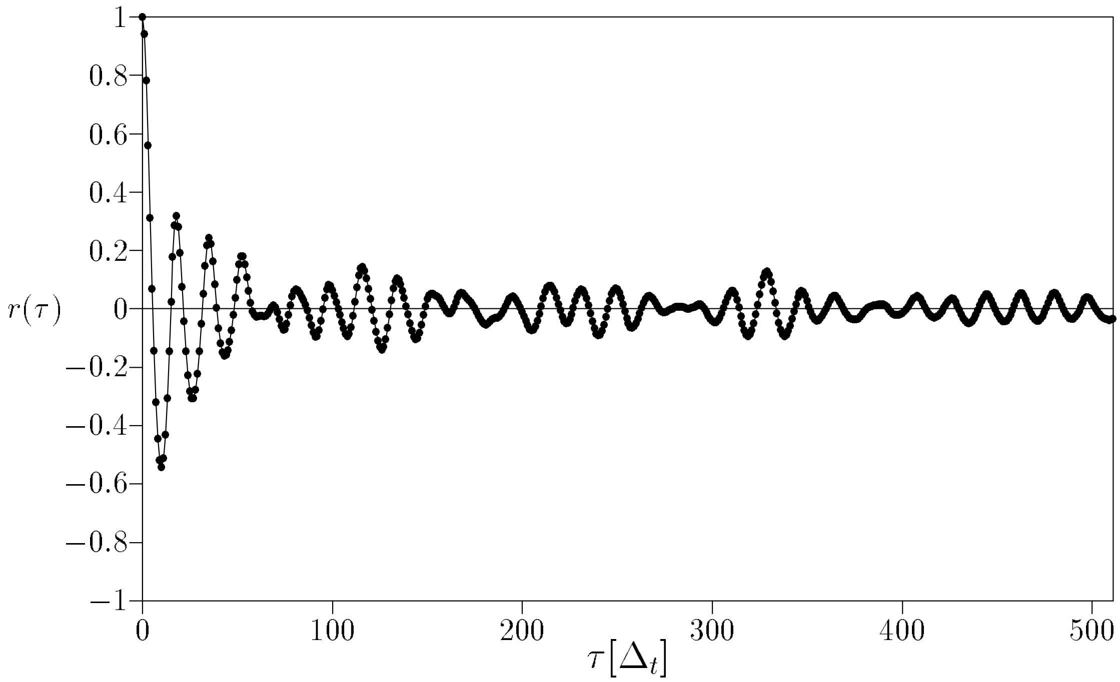

Figure 4.6: **Autocorrelation function for the set of global data for F.**
The correlations due to the periodic oscillations between the spikes decrease in the typical temporal distance between two spikes (corresponding to $\tau \approx 70 \cdot \Delta_t$*).*

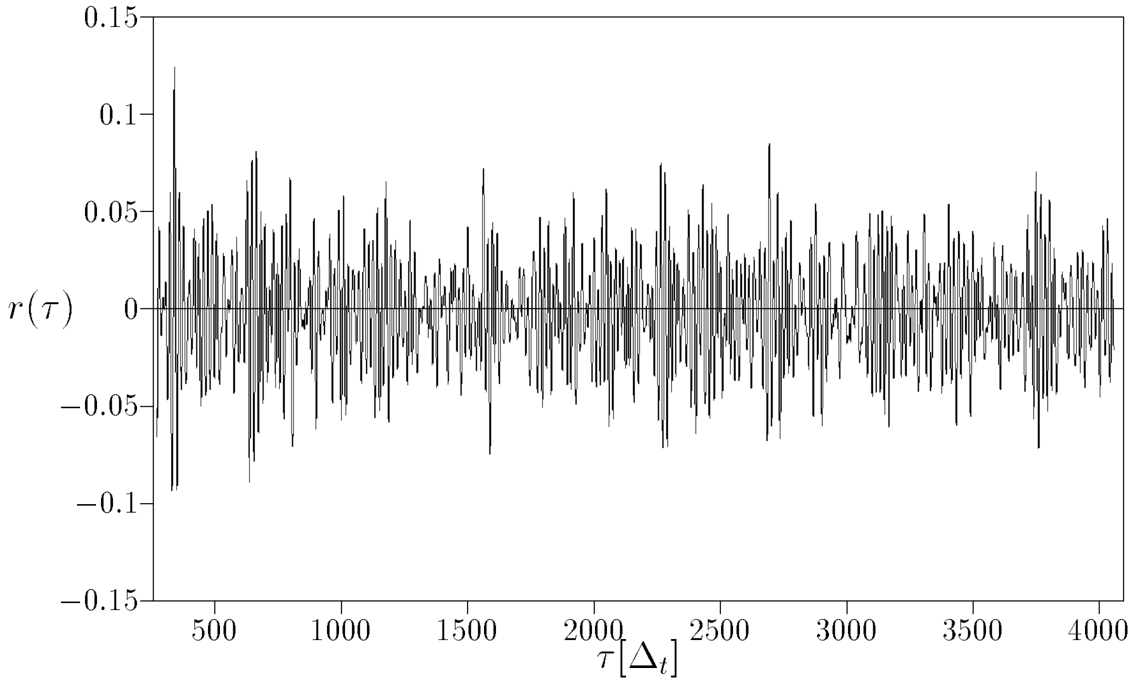

Figure 4.7: **Autocorrelation function for the set of global data for F for greater lags.**
A small correlation remains even for very long lags τ*.*

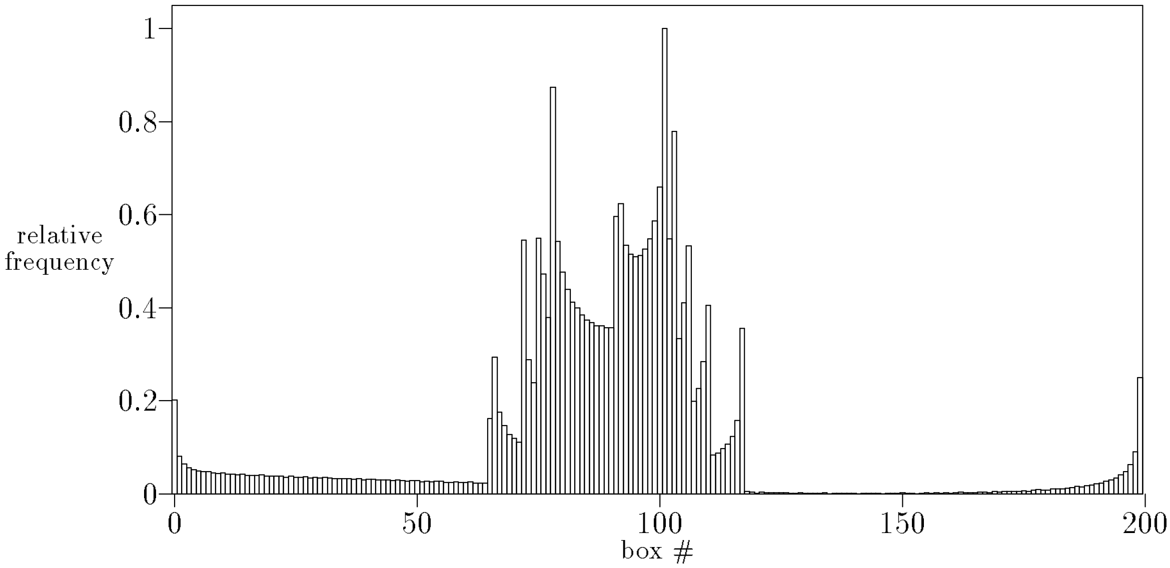

Figure 4.8: **Histogram for global data for E.**
This is a distribution statistics about the time series. The total range of all values of the time series is divided into 200 'boxes'. For each box the occurrence of time series values falling into it is counted. The values are normalized to make the greatest relative frequency equal to one.

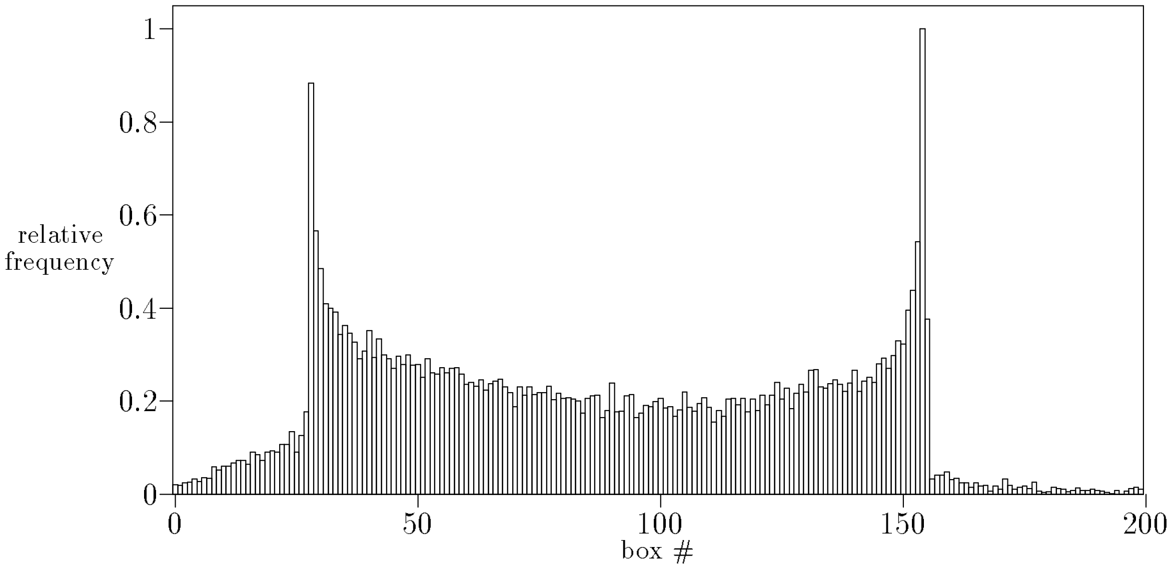

Figure 4.9: **Histogram for the global data for F.**

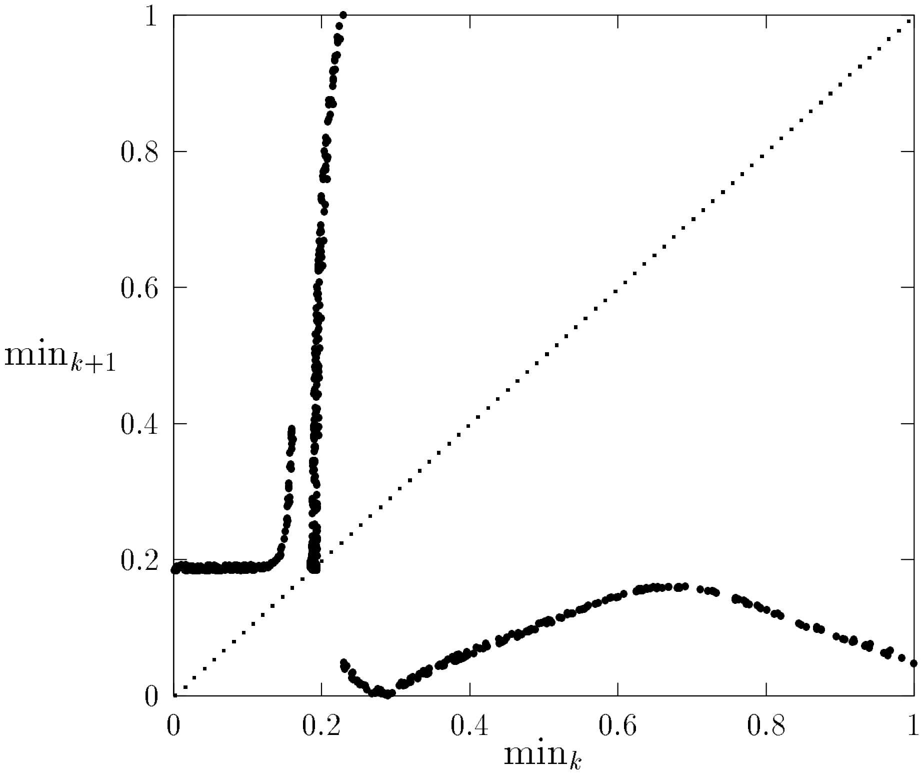

Figure 4.10: **Maximum map for the global data for F.**
For this plot the (non-interpolated) local minima were used. The dotted straight line is the curve of fixed points.

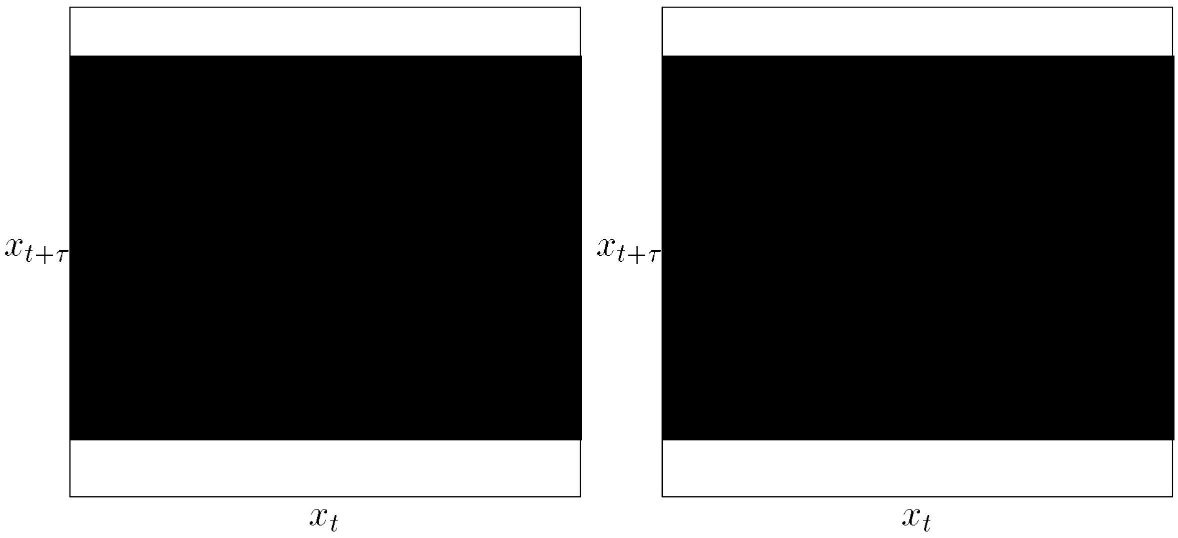

Figure 4.11: **Phase portraits for the global data set E (left) and F (right).** *(tau = $5\,\delta_t$).*

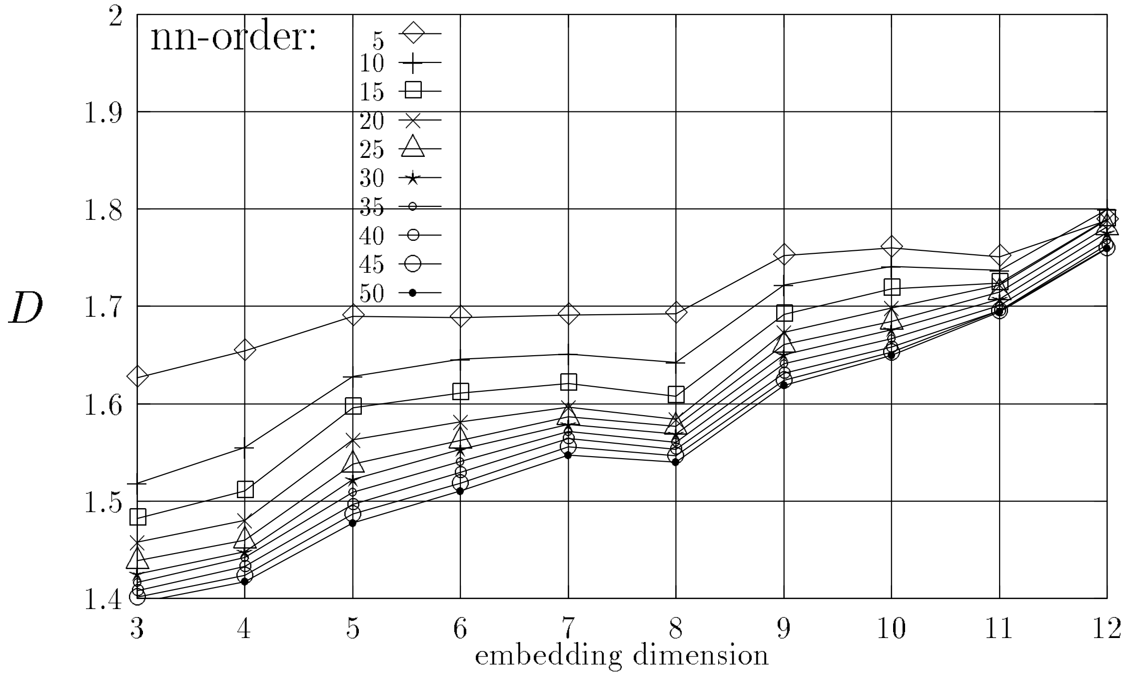

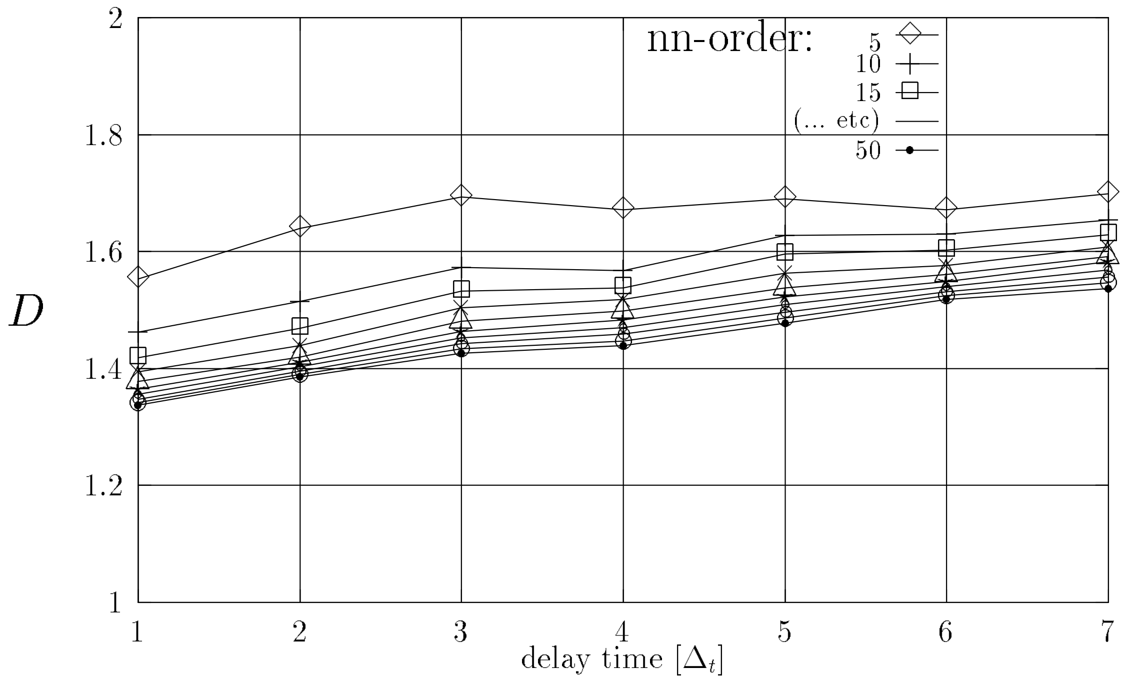

Figure 4.12: **Dimension estimates from nearest neighbor statistics for the global data set F.**
Top: results for different embedding dimensions each with delay time $\tau = 5 \cdot \Delta_t$. *Bottom: results for different delay times each with embedding dimension five. The real attractor dimension for chaotic systems must be greater two.*

4.1.3 Analysis of the Spatio-Temporal Data

Plots of the spatio-temporal data sets E and F are shown in the figures 4.13 and 4.14.

The empirical orthogonal modes for the data sets E and F were determined using the singular value decomposition. The singular values obtained for both cases are shown in table 4.2. The greatest part of the standard deviation of the data sets is already described by a few empirical modes. The first six modes together already cover more that 99.5% of the amplitude of the signal.

The empirical modes (figure 4.17) look very similar for the two cases. The scalar product between the corresponding modes gives a quantitative measure for the similarity. As can be seen in figure 4.15 the first six modes agree so much that their scalar product is greater that 0.90. The individual singular values are also quite similar for both data sets (see table 4.2). It can be deduced that the data set F corresponds to the case of purely temporal chaos.

The first mode amplitude for F (figure 4.16) indicates that the mode describes the spikes of the spatio-temporal data. The oscillations between the spiking events is described mainly by the second mode. The shape of the first and second mode (cf. figure 4.17) also suggests this correspondence.

Attractor reconstructions for data set E were made using the method of delay coordinates with the data samples from the boundary locations. For the left plot in figure 4.19 the data from the location where the spiking occurs was used. The reconstruction on the left of figure 4.18 used the data from the location opposite side of the spikes. Comparing these attractor reconstructions with reconstructions that were produced with the first (figure 4.19, right) and the second (figure 4.18, right) mode amplitude one finds a striking similarity. This again shows that the first two modes can be assigned to the different parts in the spatio-temporal dynamics. On the other hand this illuminates the fact that for a system with spatially perfectly coherent dynamics the properties can be drawn from time series that are simply the data values at one location[11]. This is not only the case for the temporal periodic data set E.

The attractor reconstructions for data set F produced with the analogous data (figures 4.21 and 4.20) show the same similarities. The form of the attractor reconstructions from the global data (for E and F, cf. figure4.11) also looks quite similar to those above.

The attractor reconstruction from the higher mode amplitudes (figure 4.22 and 4.23) tend to be more and more 'knotted'. Their forms do not reflect physically interesting properties but result from the orthogonality property of the empirical modes and their amplitudes.

The fact that the first few empirical modes already cover more than 99% of the dynamics and that almost the 'same' individual modes are found for both the case of periodic behavior and the case of temporal chaos strongly suggests that a Galerkin projection should be made for this system. This idea is also supported by the fact that there are no

[11] There may be 'pathological' locations that cannot be used.

parts in the dynamics that occur only rarely[12].

The procedures for the estimation of attractor dimension and Lyapunov exponents used for the global data sets also fail if the data of the mode amplitudes is used. With the amplitudes of the different modes and different parameter values for embedding and delay time one also obtains spurious results. This may be attributed to the strong nonuniformity of the attractor. The dominance of the periodic regime may be responsible for the deviation of the dimension estimates towards values which are too low.

[12]This would mean that also modes with small corresponding singular values would have to be used for the projection.

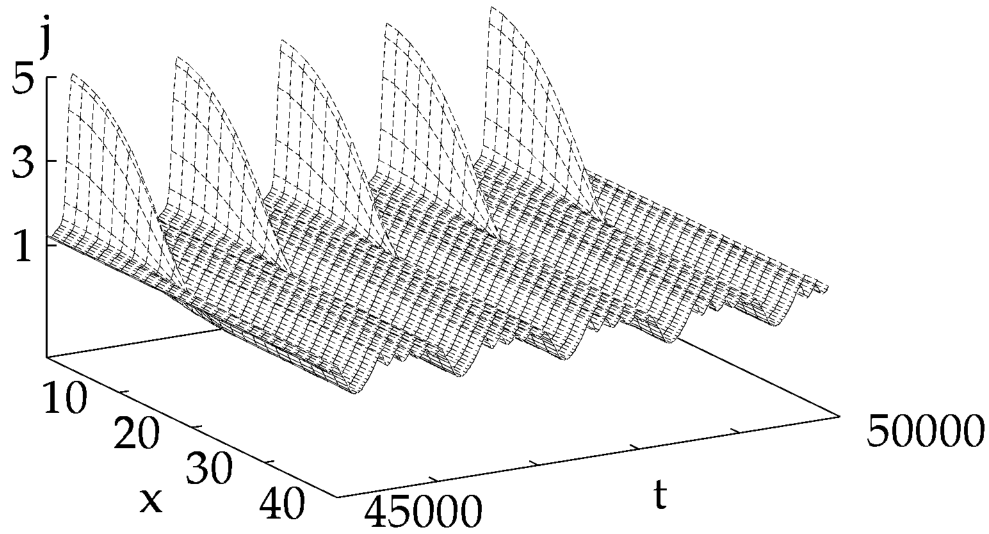

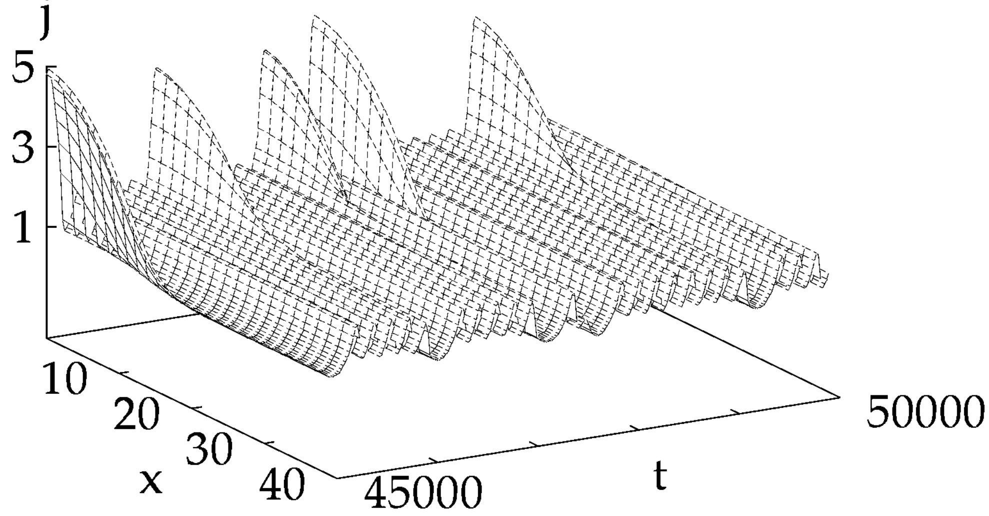

Figure 4.14: **Spatio-temporal dynamics of system F.**

	singular values (sum=100%)		cumulative singular values	
#	data set E	data set F	data set E	data set F
1	65.981894	56.000767	65.981894	56.000767
2	22.987449	30.938192	88.969343	86.938959
3	6.8527171	7.7839196	95.82206	94.722878
4	2.2522257	2.932187	98.074286	97.655065
5	1.0648752	1.2767171	99.139161	98.931782
6	0.46774304	0.57862294	99.606904	99.510405
7	0.20435136	0.24799574	99.811255	99.758401
8	0.0990691	0.12110195	99.910324	99.879503
9	0.04599989	0.05907286	99.956324	99.938576
10	0.02166702	0.02929208	99.977991	99.967868

Table 4.2: **The first singular values (left) and cumulative singular values (right) for E and F.** *They are normalized to add up to* 100%. *Each singular value tells how much of the standard deviation of the original data is described by the corresponding empirical mode. The cumulative value at number k tells how much of the standard deviation of the original data is described by the all empirical modes up to mode number k. Here few empirical modes suffice to cover more than* 99% *of the amplitude.*

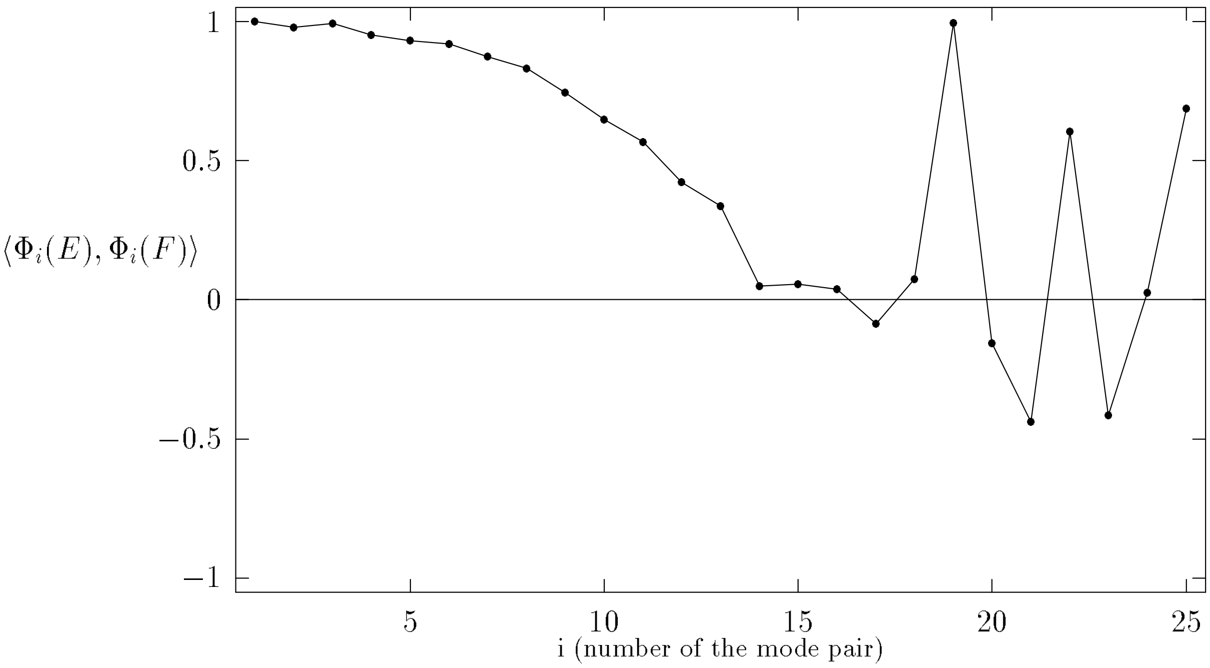

Figure 4.15: **The scalar products of the modes for data sets E and F.** *$\Phi_i(E)$ and $\Phi_i(F)$ denote the empirical mode number i for data sets E and F respectively. The first six modes that cover in both cases more than* 99.5% *of the amplitude have scalar products greater than* 0.9.

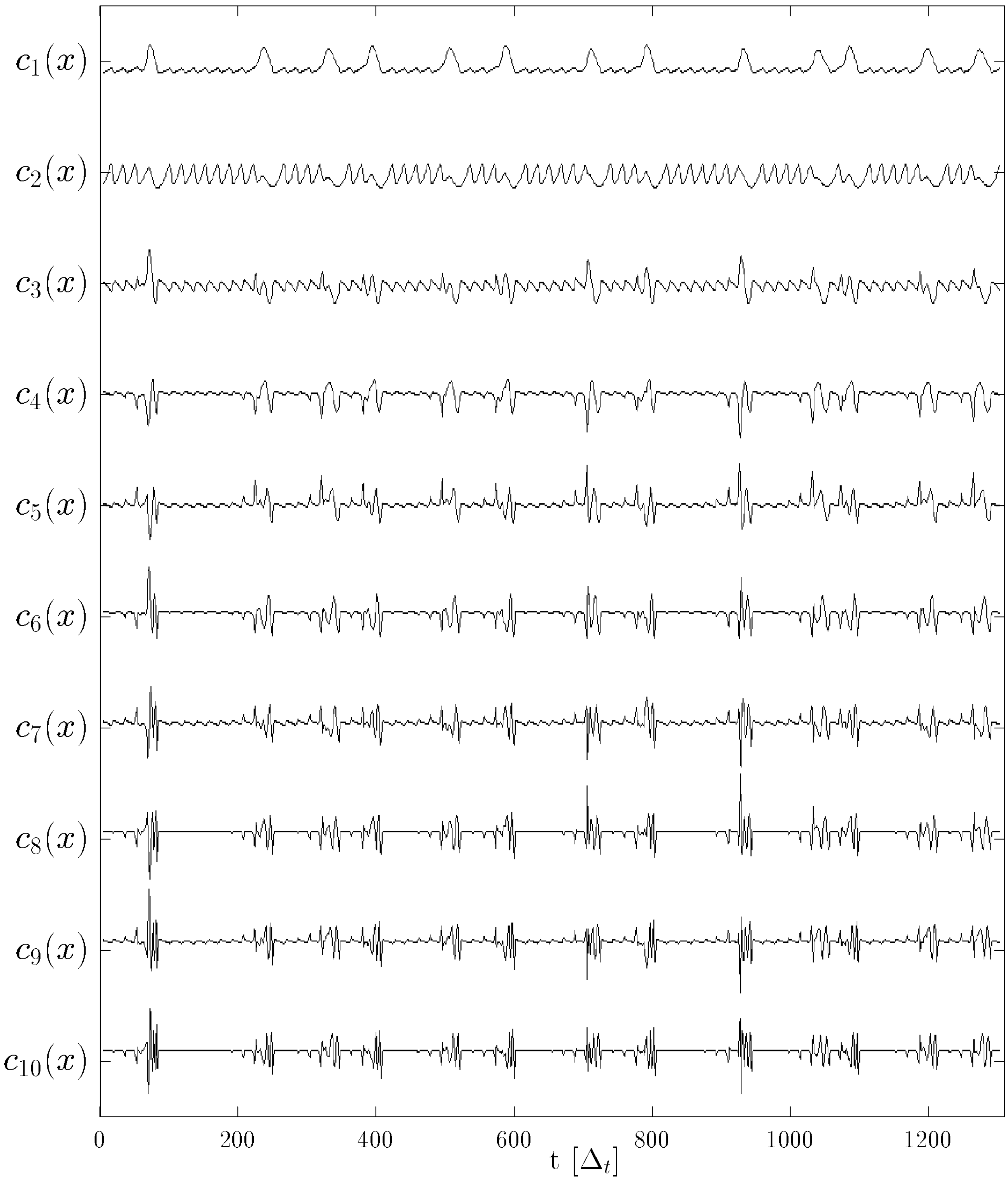

Figure 4.16: **The first ten mode amplitudes $c_k(t)$ for data set F.**
Each mode amplitude is a vector of norm one.

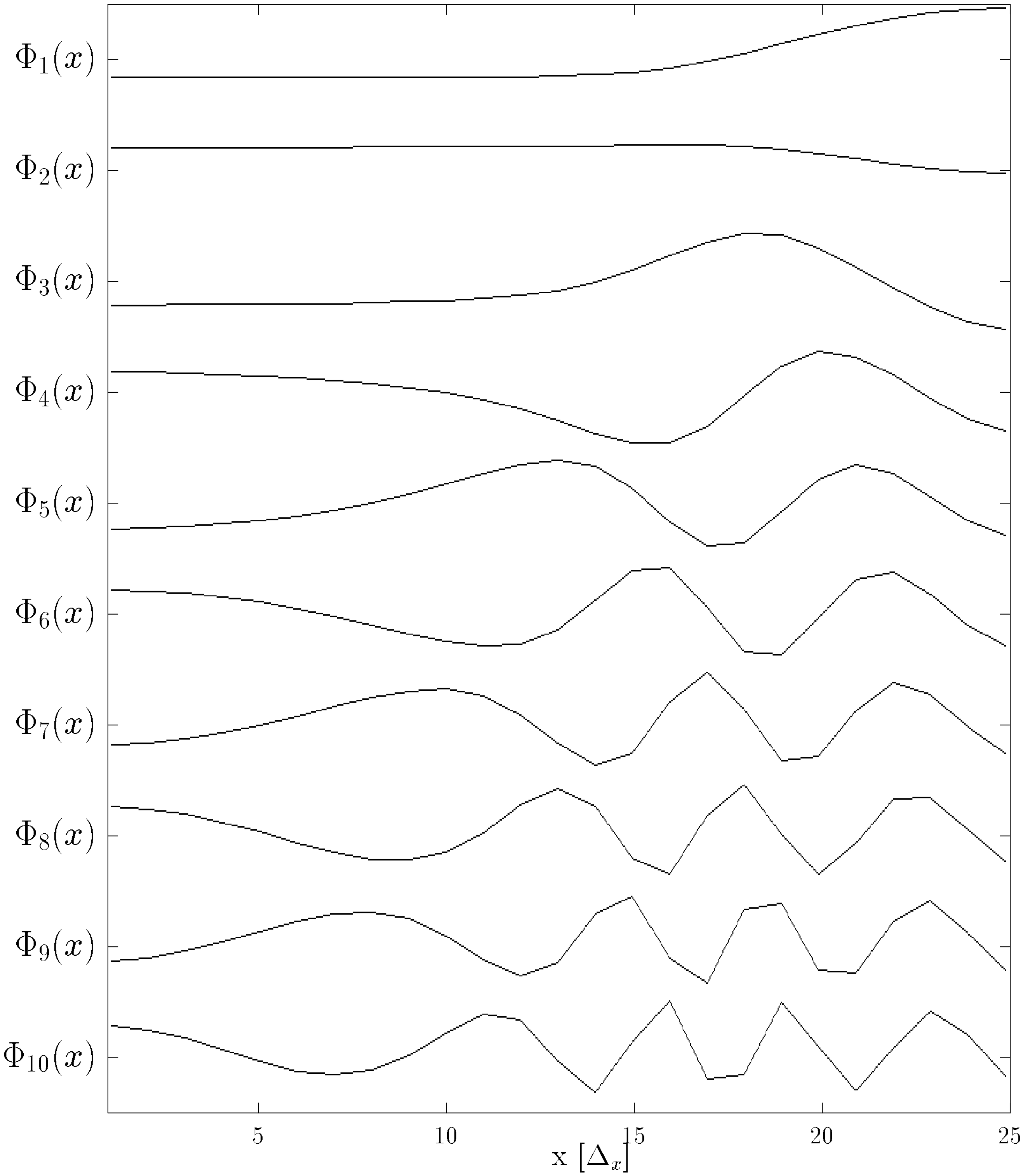

Figure 4.17: **The first ten empirical modes $\Phi_k(x)$ for data set E (drawn with points) and F.**
Each mode is a vector of norm one.

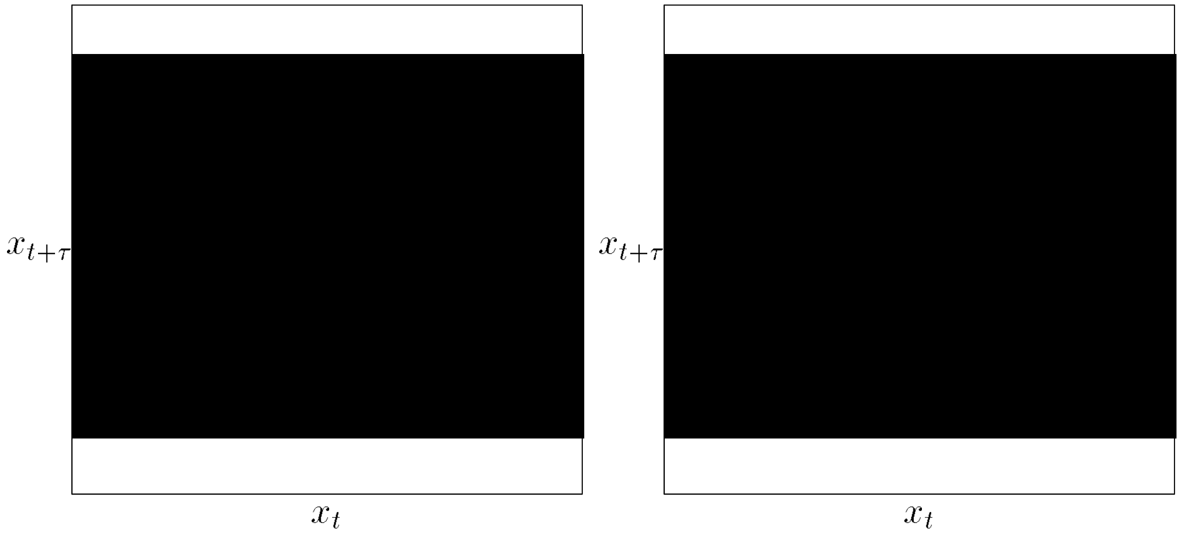

Figure 4.18: **Phase portraits for data set E: for the spatial location opposite to the spikes (left) and for the second modeamplitude (right).** *(delay $\tau = 5\,\Delta_t$).*

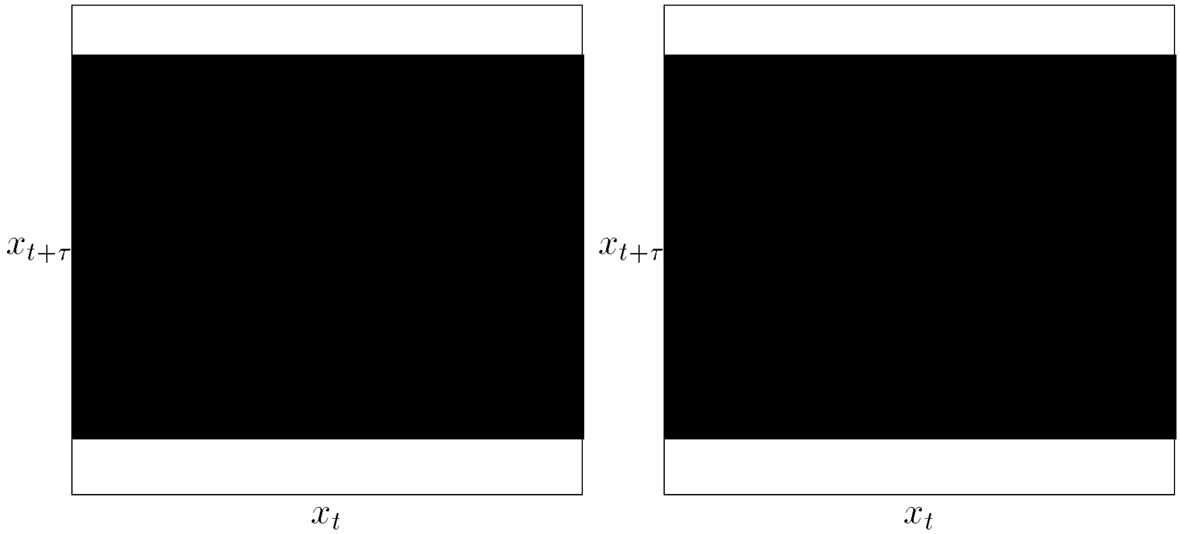

Figure 4.19: **Phase portraits for data set E: for the spatial location of the spikes (left) and for the first modeamplitude (right).** *(delay $\tau = 5\,\Delta_t$).*

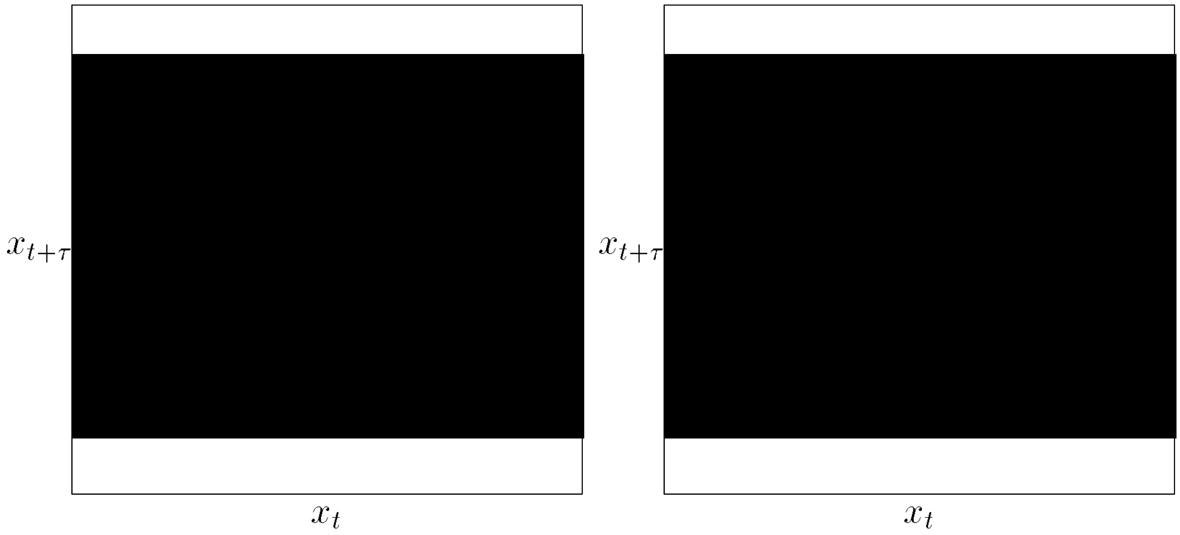

Figure 4.20: **Phase portraits for data set F: for the spatial location opposite to the spikes (left) and for the second modeamplitude (right).** *(delay $\tau = 5\,\Delta_t$).*

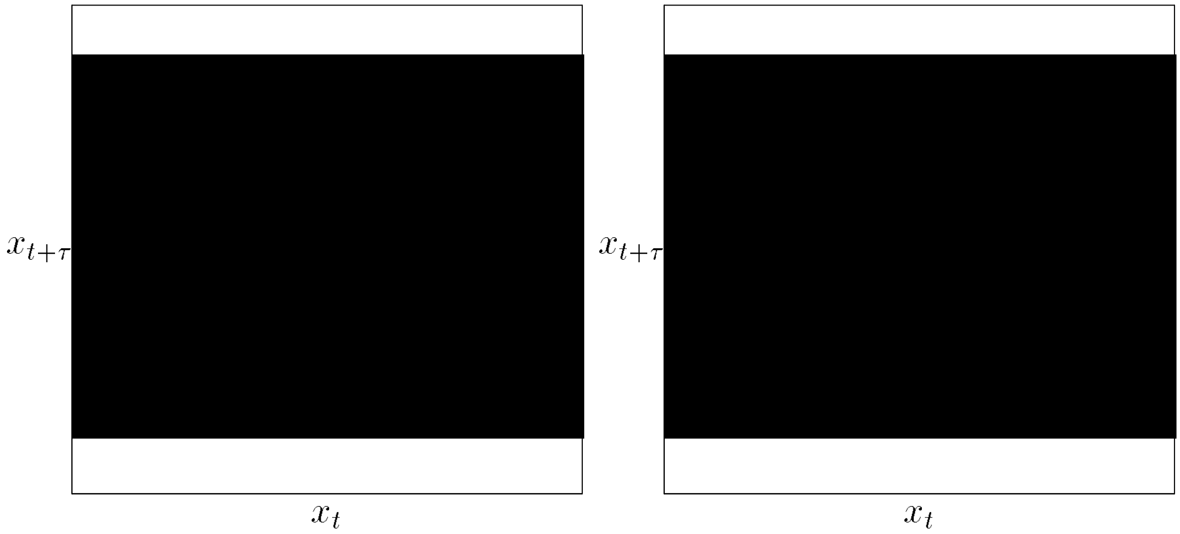

Figure 4.21: **Phase portraits for data set F: for the spatial location of the spikes (left) and for the first modeamplitude (right).** *(delay $\tau = 5\,\Delta_t$).*

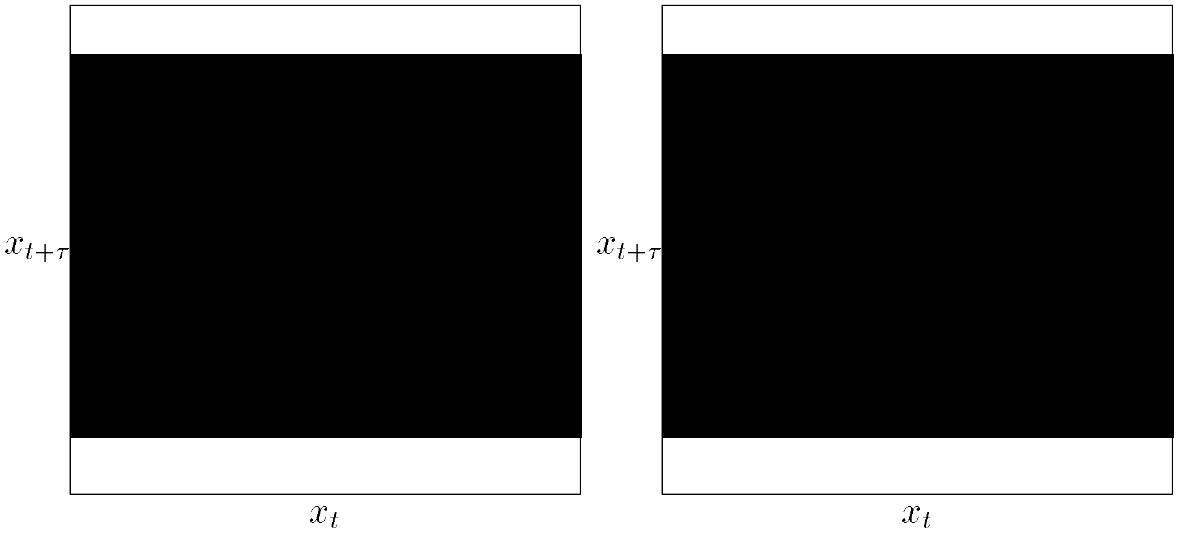

Figure 4.22: **Phase portraits for the third (left) and the fourth (right) mode amplitude of data set E.** *(delay $\tau = 5\,\Delta_t$).*

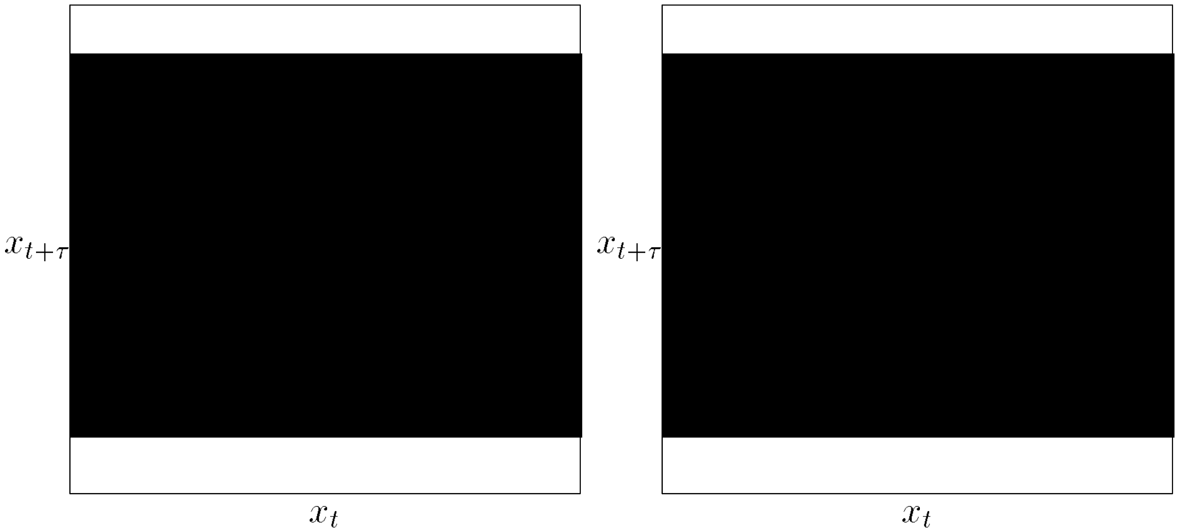

Figure 4.23: **Phase portraits for the fifth (left) and the sixth (right) mode amplitude of data set E.** *(delay $\tau = 5\,\Delta_t$).*